Supplementary Information

S1: Experimental

S1.1: Materials

Aqueous solutions of nitric acid (65 %, Merck) and ammonium hydroxide (25 %, Merck) were used as received. Sodium hydroxide pellets (98 %, PanReac AppliChem) were dissolved in deionized water to produce sodium hydroxide solutions. Silver and copper precursors were obtained as solid silver nitrate ($AgNO_3$, >99 %) and copper nitrate ($Cu(NO_3)_2$, >99.99 %) from Sigma Aldrich. As catalyst support materials titanium dioxide (TiO_2, Aeroxide P25) from Acros Organics, fumed silica (SiO_2, mean particle size 0.2 to 0.3 µm) and zirconium dioxide (ZrO_2, 99 % trace metal basis, mean particle size 5 µm) both from Sigma Aldrich were used. Methanol (>99.8 %) was obtained from Merck and nitrogen (99.999 %) and synthetic air were purchased from Air Liquide. Deionized water was used throughout the experiments.

S1.2: Catalyst synthesis

The pH_{PZC} of each support was determined by adapting a procedure described by Park and Regalbuto.[1] Dilution series from pH 1 to 13 were prepared from 1 M sodium hydroxide solution and 1 M nitric acid solution. Values of pH were measured with an Inolab pH7310 (WTW). For each pH value, the amount of support material to achieve a concentration of support surface area (CSA) of 1000 m²/L was weighed and prepared in a 200 ml flask. Afterwards, the flask was filled up with the respective solution and shaken with an orbital shaker at 170 rpm for one hour. The suspension was then centrifuged for 15 min at 10000 rcf. The solid was separated and the pH of the solution was determined. For PZC determination, the final pH value was plotted as a function of the initial pH value.
The metal precursor solutions (200 ppm) were prepared by dissolving the respective nitrates.[2,3] To prepare a silver diammine (AgDA) solution (200 ppm), $AgNO_3$ (0.315 g) was dissolved in water (100 mL). By dropwise addition of NaOH (450 µL, 5 M), solid silver oxide was formed and then dissolved to form AgDA by adding ammonium hydroxide solution (750 µL). The colorless solution was diluted with water to a volume of one liter. The final pH value of the AgDA solution was 11.6. Due to the light sensitivity of silver, all glass vessels were covered with aluminum foil. To synthesize a copper tetraammine (CuTA) solution (200 ppm), $Cu(NO_3)_2$ (0.732 g) was dissolved in water (100 mL). Ammonium hydroxide solution (28 mL) was added, and the solution was diluted with water to one liter. The final pH value was 11.5.

S1.3: Characterization

The metal uptake by the support material was determined by measuring the metal concentration in the solution before and after SEA with inductively coupled plasma – optical emission spectroscopy (ICP-OES) (ICP-OES 700 series, Agilent Technologies). A sample flow of 1.3 ml/min and a frequency of 40 MHz at the induction coil was used. For calibration, certified calibration standards were purchased as 1000 ppm $AgNO_3$ in nitric acid from Merck and 1000 ppm $Cu(NO_3)_2$ in nitric acid from Carl Roth. A three-point calibration series of 0.1 ppm, 1 ppm and 5 ppm was prepared by diluting with 0.2 M HNO_3.

S2: Results

S2.1: pH_{PZC} of the support materials

The measured pH_{PZC} values for silica and zirconia were in good agreement with previous reports.[3,4] For titania, the determined pH_{PZC} was within the range of previously reported pH_{PZC} values. For example, Machado and coworkers determined a pH_{PZC} of 3.5 for TiO_2 (P25),[5] while Zeng et al. measured a pH_{PZC} of 5.2 for titania (P25) but 6.1 for pure anatase.[6] Production dependent differences in crystal structure and their effect on the pH_{PZC} have been observed for TiO_2. The pH_{PZC} of fumed silica could be reduced when removing alkali impurities by washing with nitric acid.[3] In case of zirconia, changes in measured pH_{PZC} values were also observed and related to differences in morphology, production procedure or pretreatment techniques.[7] In general, all pH_{PZC} values for the support materials were within the acidic regime and suitable for adsorption of positively charged metal complexes *via* SEA under moderate conditions.

S2.2: UV-vis spectra of the metal precursor solutions

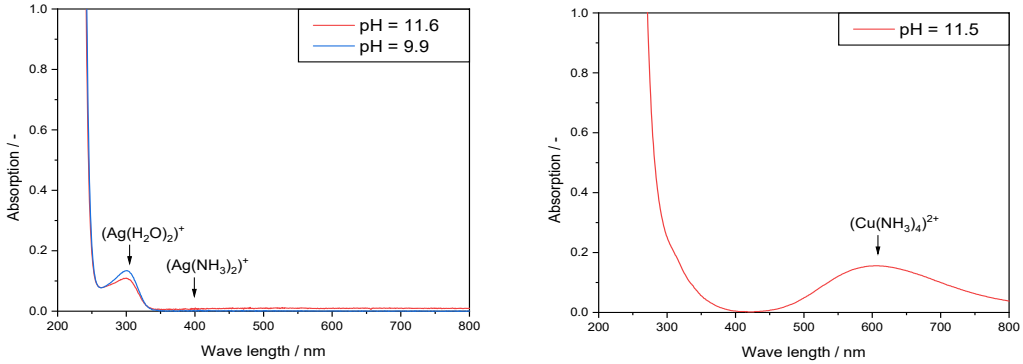

Figure S1: UV-vis spectra for AgDA solution (left) and CuTA solution (right). At pH 11, the molar fraction of the diammine complex was reported to be larger than 95 % (the presence of some $[Ag(H_2O)_2]^+$ is indicated here by the band at 300 nm). Note that the extinction coefficient of the $[Ag(NH_3)_2]^+$ complex is very small and the complex reveals only a very weak and very broad band at 400 nm, while the $[Ag(H_2O)_2]^+$ complex is observed as a strong band at 300 nm with a much higher extinction coefficient.

S2.3: STEM-HAADF images and elemental maps

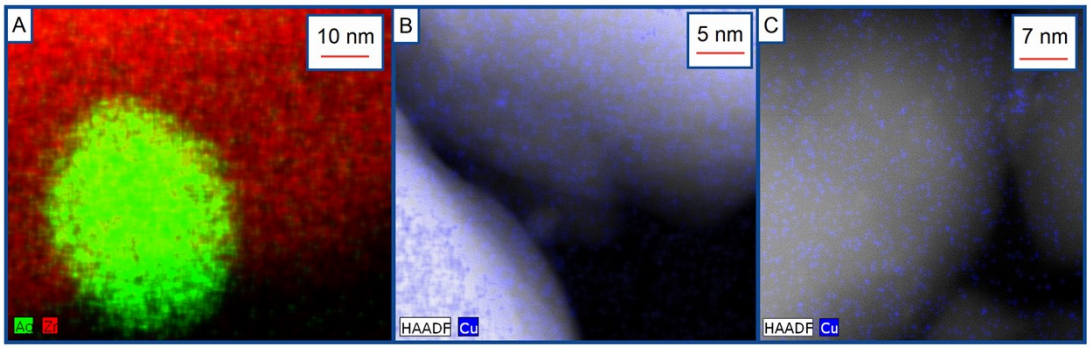

Figure S2: Elemental maps obtained from STEM-EDX spectrum imaging of the catalysts (A: Ag/ZrO_2 1000 m²/L, B: Cu/ZrO_2 1000 m²/L, C: Cu/TiO_2 1000 m²/L

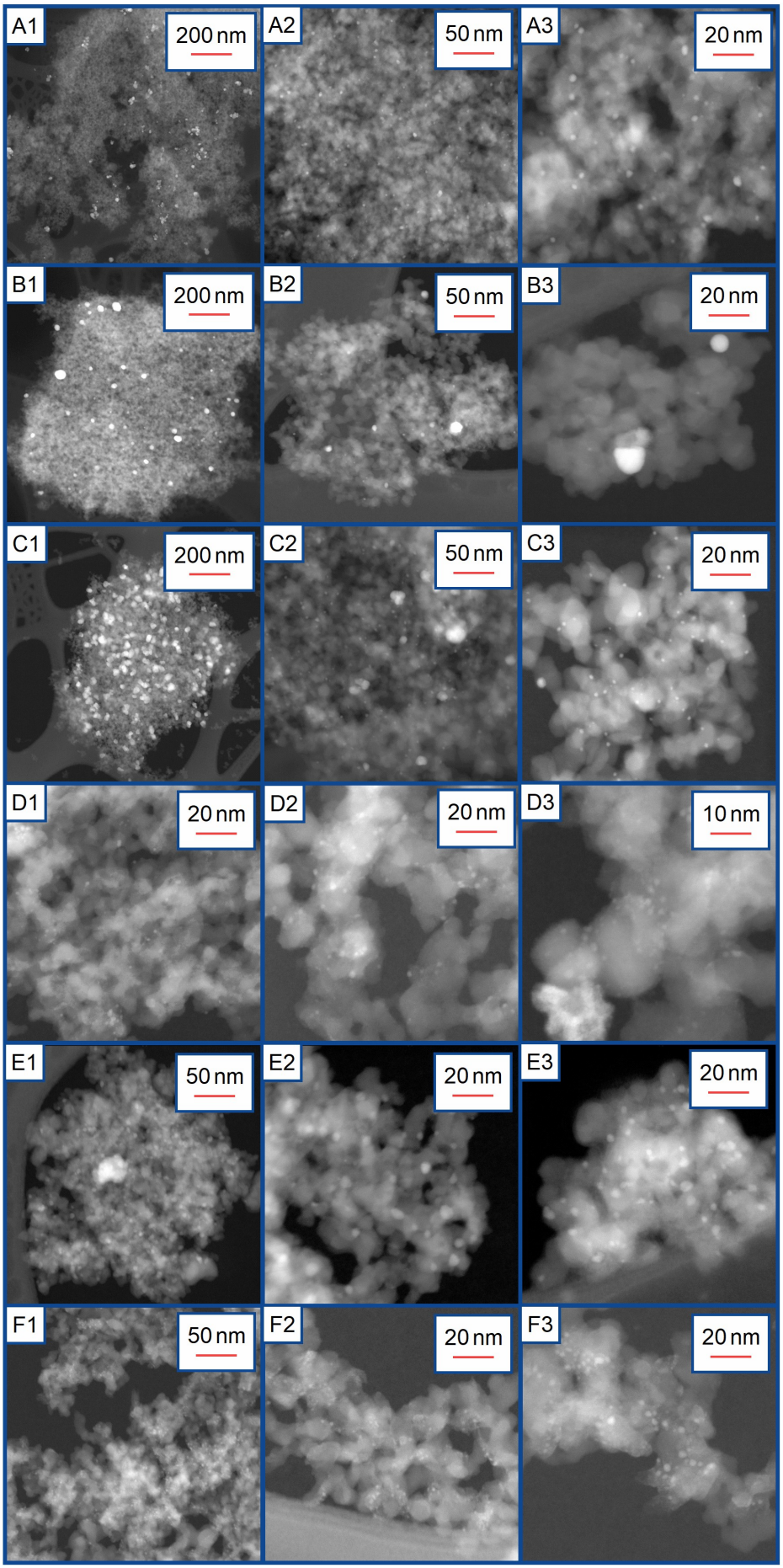

Figure S3: STEM-HAADF images of the catalysts (A: Ag/SiO_2 1000m²/L, B: Ag/SiO_2 1000m²/L after reaction, C: Ag/SiO_2 2x500m²/L. D: Cu/SiO_2 1000m²/L, E: Cu/SiO_2 1000m²/L after reaction, F: Cu/SiO_2 2x500m²/L)

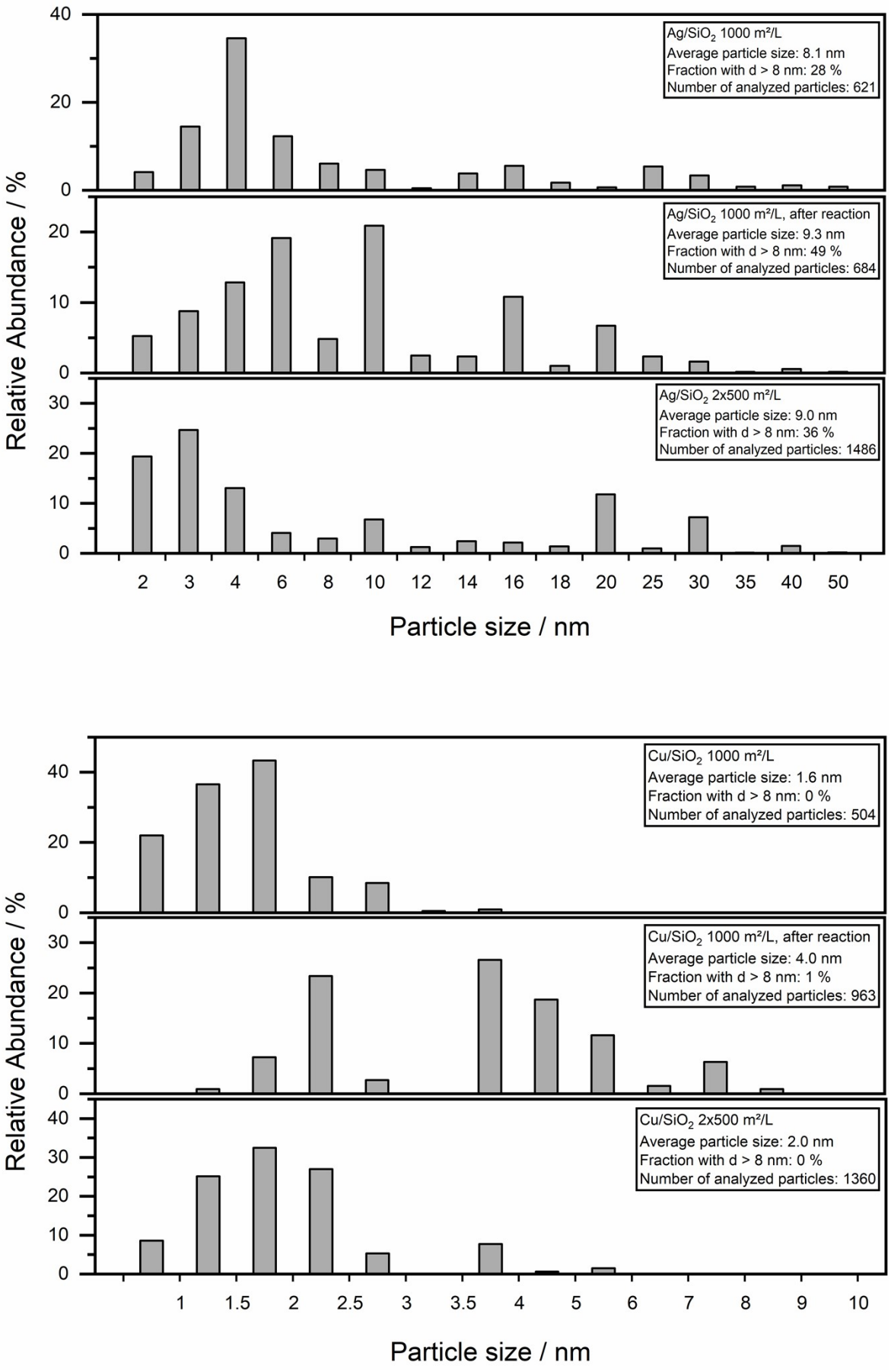

Figure S4: Particle size distribution for Ag/SiO_2 catalysts (top) and Cu/SiO_2 catalysts (bottom)

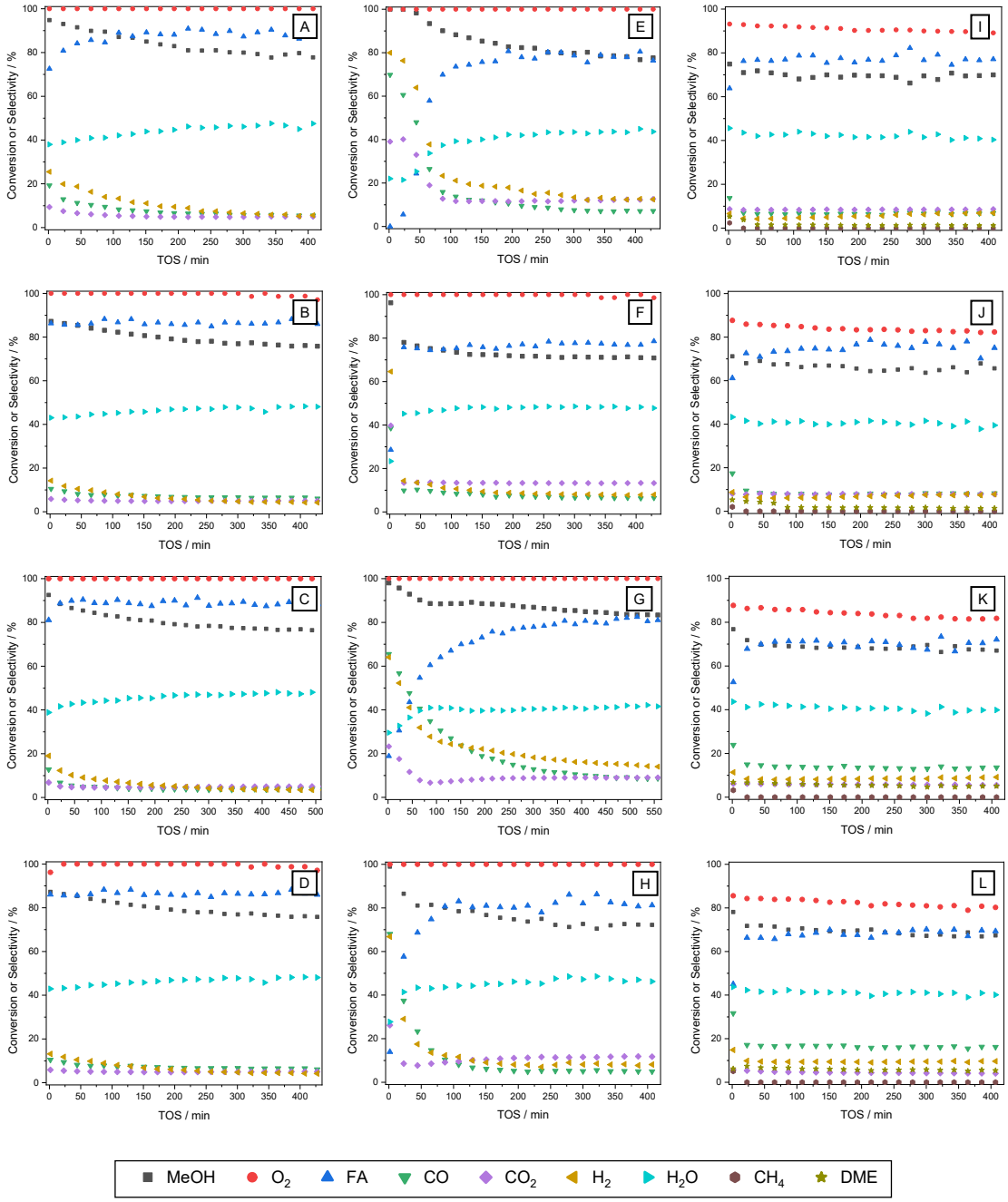

Figure S5: Conversion and selectivity as function of time on stream for Ag/SiO_2 (A: 500 m²/L, B: 2000 m²/L, C: 4000 m²/L, D: 2x500 m²/L), Cu/SiO_2 (E: 500 m²/L, F: 2000 m²/L, G: 4000 m²/L, H: 2x500 m²/L), Ag/TiO_2 (I: 500 m²/L, J: 2000 m²/L, K: 4000 m²/L, L: 2x500 m²/L). Feed: 2.5 % methanol and 1.0 % oxygen in nitrogen, total flow rate: 1 L_{STP}/min, reaction temperature: 575 °C.

S2.4 Catalytic testing

S3: Additional experimental studies and discussion

S3.1: Influence of catalyst pretreatment and temperature-dependent activity-selectivity trends

Prior to the catalytic tests, the catalysts were calcined in the flow reactor using the following procedure: 1) heating in synthetic air to 575 °C (0.5 L_{STP}/min, 15 °C/min) and 2) 15 min at 575 °C. To study the influence of the reaction temperature on conversion and selectivity, the temperature was stepwise increased every hour by 25°C until a temperature of 650°C was reached (feed: 2.5 % methanol and 1.0 % oxygen in nitrogen, total flow rate: 1 L_{STP}/min). Prior to these experiments, all samples were kept for 8 hours at 500°C to achieve steady-state activity under constant reaction conditions (i.e., 2.5 % methanol and 1.0 % oxygen in nitrogen, 1 L_{STP}/min total flow rate). Figures S6 A and C show the catalyst tests for Ag/SiO_2 and Cu/SiO_2 under the same reactions conditions as shown in Figures 3 A and D of the manuscript, respectively, demonstrating the high reproducibility of the observed temperature-dependent trends for conversions and selectivities.

The same catalysts were also pretreated at 650 °C using the above procedure. Figures S6 B and D show the temperature-dependent catalytic behavior for Ag/SiO_2 and Cu/SiO_2 after pretreatement at 650°C, respectively. The temperature-dependent conversions and selectivities in methanol ODH were the same as for catalyst pretreatment at 575°C demonstrating that the observed temperature-dependent activity-selectivity trends were independent of the catalyst pretreatment temperature in the investigated temperature range.

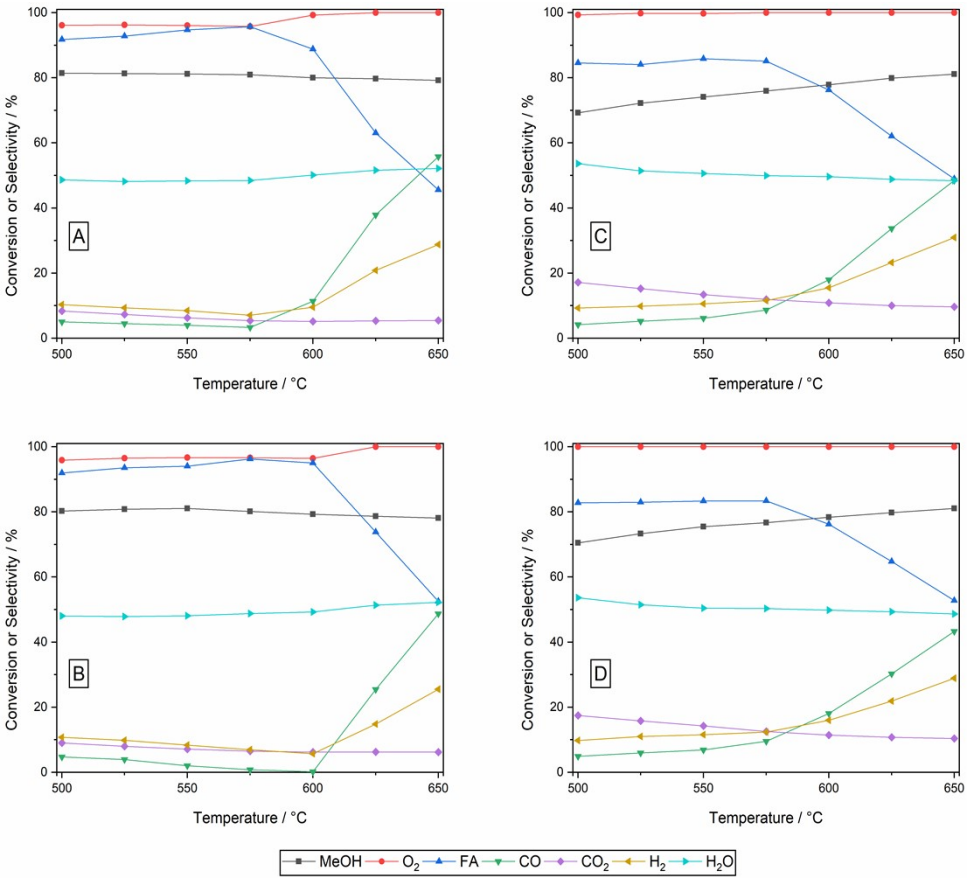

Figure S6 Conversion and selectivity as a function of the temperature for Ag/SiO_2 calcined at 575 °C (A) and 650 °C (B) and Cu/SiO_2 calcined at 575 °C (C) and 650 °C (D) with CSA = 1000 m²/L in all cases (feed: 2.5 % methanol and 1.0 % oxygen in nitrogen, total flow rate: 1 L_{STP}/min).

S3.2: Activity of titania and zirconia support material

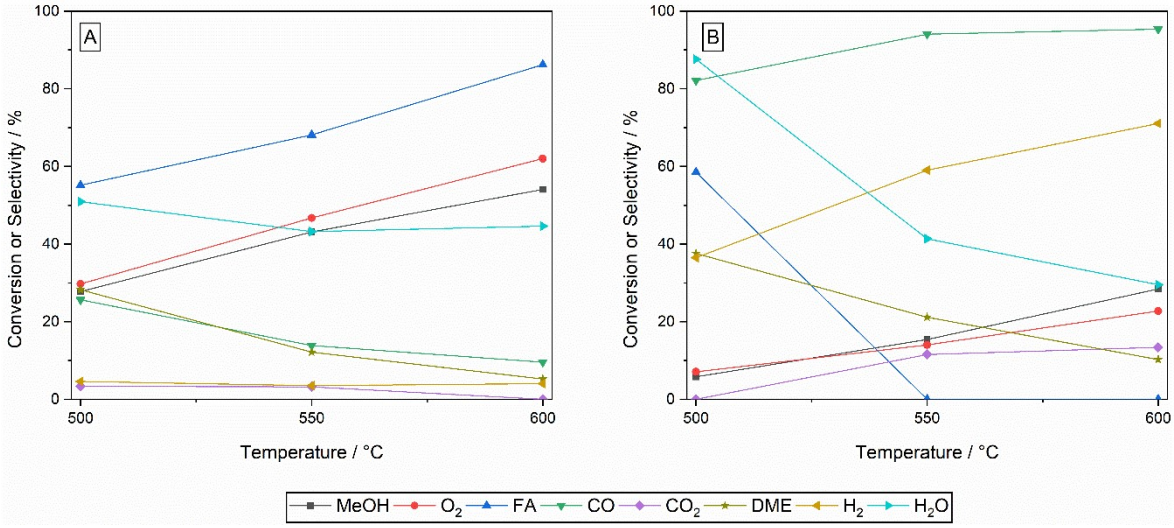

Figure S7 Conversion and selectivity as a function of the temperature for the support materials, TiO_2 (A) and ZrO_2 (B) (feed: 2.5 % methanol and 1.0 % oxygen in nitrogen, total flow rate: 1 L_{STP}/min, TOS: 4 h).

S3.3: Influence of the metal loading on methanol conversion and selectivity

To further support the conclusions on the influence of the silver loading on methanol conversion and product selectivities, a number of additional catalytic tests was performed using the series of Ag/SiO_2 catalysts (i.e. with silver loadings of 0.58, 1.15, 1.53, 3.43, and 3.86 wt%). For each catalyst, also different methanol feed fractions were applied (i.e. 2.2, 2.6 and 3.7 mol%), while the methanol to oxygen ratio was 2.4, the total flow rate was 1 L_{STP}/min and the reaction temperature was 575 °C. Figures S9 A – C display the reactant conversions and product selectivities as a function of the silver loading of the catalyst for 2.2 mol% (A), 2.6 mol% (B) and 3.7 mol% methanol (C) in the feed. For 2.2 mol% methanol in the feed, the increase in methanol conversion with higher silver loadings was readily apparent. The overall methanol conversion did not decrease (nor increase) for increase of methanol in the feed to 2.6 mol% and 3.7 mol%, respectively, and the same trends were observed. Hence, a lack of active sites may be excluded as a reason for this increase in methanol conversion observed for increase in the silver loading (see also Figure 5 in the manuscript). In all cases, the increase in methanol conversion over silver loading was accompanied by an increase in H_2 selectivity, while the H_2O selectivity decreased. Since the CO selectivity did not reveal the same trend, the decomposition of FA could not be responsible for the additional formation of hydrogen. Thus, hydrogen should be formed in the catalytic reaction. A change in the relative abundance of oxygen species (i.e., an increase in the O_γ to O_α ratio) could increase the probability of methoxy species decomposition and thereby lead to a higher methanol conversion. In this case, a parallel increase in hydrogen formation (due to higher probability of hydrogen atom recombination) would be a side effect. This is consistent with an increase in H_2 selectivity with increasing silver loading, as observed in the experiments. These results and trends are consistent with the experiments shown in Figure 5 of the manuscript (which are extracted in Figure S8 for better illustration), demonstrating the high reproducibility of the results and trends observed in these experiments.

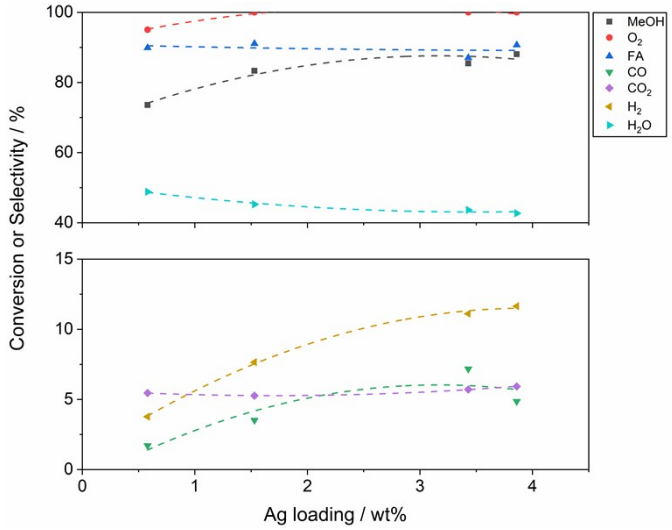

Figure S8: Conversions and selectivities for Ag/SiO_2 catalysts as a function of the metal loading for 2.2 mol% methanol in the feed (methanol-oxygen ratio: 2.4, total flow rate: 1 L_{STP}/min, reaction temperature: 575 °C, TOS: 8 h). The data were extracted from Figure 5 of the manuscript.

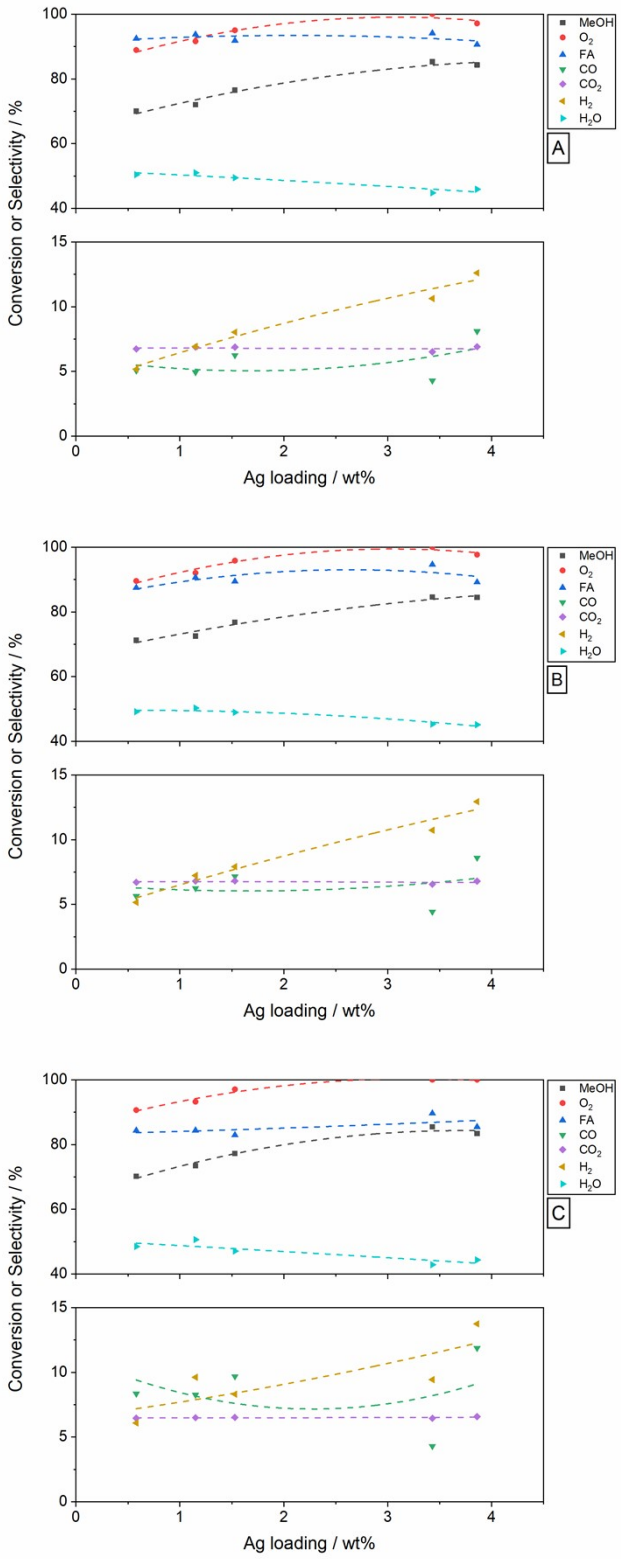

Figure S9: Conversions and selectivities for Ag/SiO_2 catalysts as a function of the metal loading for 2.2 mol% methanol (A), 2.6 mol% methanol (B) and 3.7 mol% methanol (C) (methanol-oxygen ratio: 2.4, total flow rate: 1 L_{STP}/min, reaction temperature: 575 °C, TOS: 8 h).

S3.4: XRD patterns of the Ag/ZrO_2, Cu/ZrO_2 and Cu/TiO_2 catalysts after the catalytic reaction

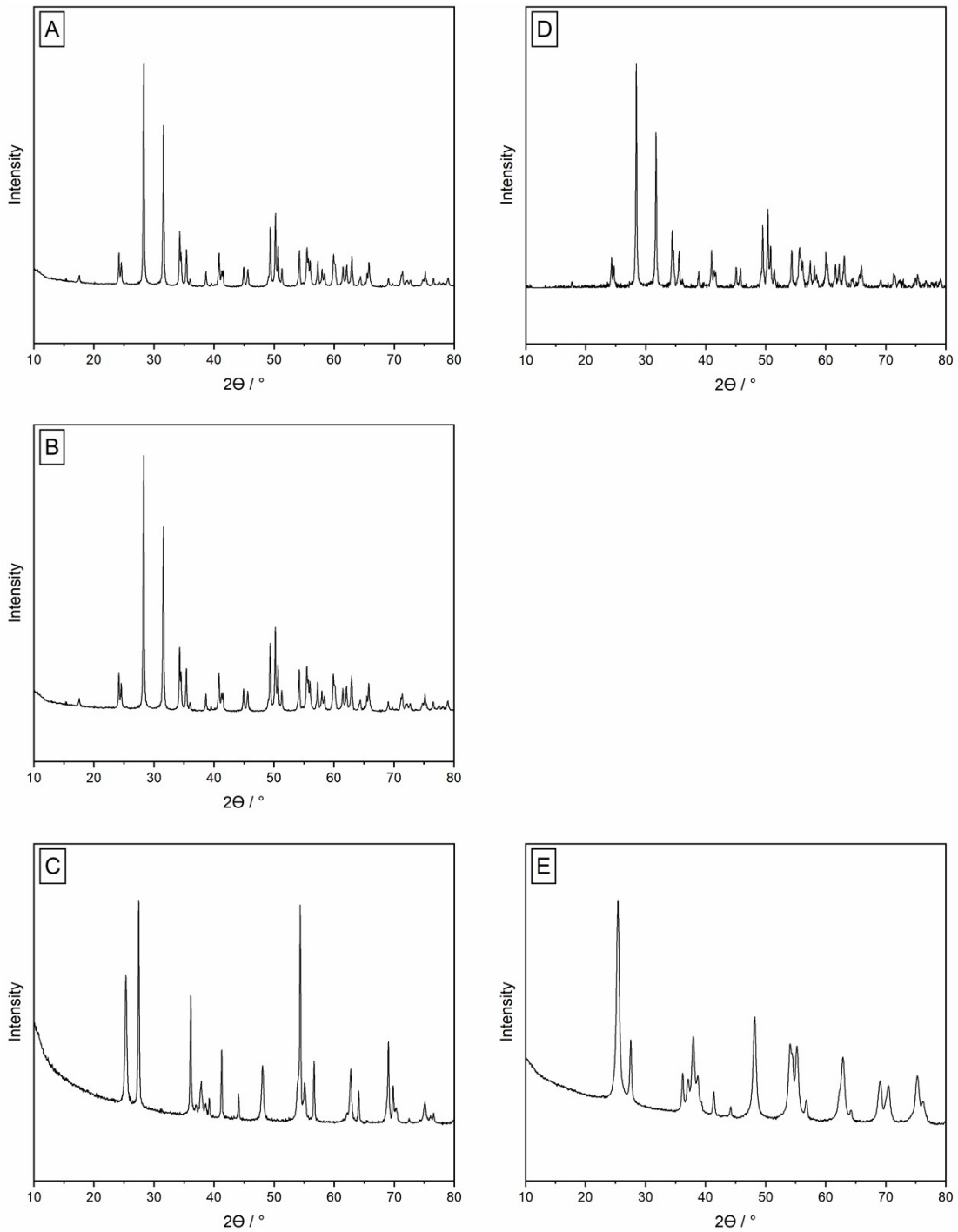

Figure S10 XRD patterns of zirconia supported catalysts (A: Ag/ZrO_2 1000 m²/L, B: Cu/ZrO_2 1000 m²/L) and titania-supported catalysts (C: Cu/TiO_2 1000 m²/L) after the catalytic reaction. The patterns of the pure support materials are illustrated in graphic D (ZrO_2) and E (TiO_2).

The XRD patterns of the Ag/ZrO_2, Cu/ZrO_2 and Cu/TiO_2 catalysts reveal the characteristic reflections of the ZrO_2 and TiO_2 phase. It should be noted that a partial phase transition occurs for the TiO_2 support from anatase to rutil under the conditions of catalyst testing. This is in good agreement with the Ag/TiO_2 catalyst after catalytic reaction (see also main manuscript). As a consequence of small particle sizes and / or low metal loadings, the XRD patterns do not reveal any reflections of the Ag or Cu phase (for more details of the catalyst

characteristics see also Table 1 in the main manuscript). This is supported by STEM-HAADF images and elemental maps, e.g., for the Cu/ZrO_2 and Cu/TiO_2 catalysts (see Figure S2 in the SI) where Cu species revealed sizes well below 2 nm.

References

1 J. Park and J.R. Regalbuto, *J. Colloid and Interf. Sci.*, 1995, 175, 239–252.
2 M. Zienkiewicz-Strzałka, S. Pasieczna-Patkowska, M. Kozak and S. Pikus, *Appl. Surf. Sci.*, 2013, 266, 337–343.
3 L. Jiao and J.R. Regalbuto, *J. Catal.*, 2008, 260, 329–341.
4 N.C.S. Selvam, A. Manikandan, L.J. Kennedy and J.J. Vijaya, *J. Colloid and Interf. Sci.*, 2013, 389, 91–98.
5 N.R.C. Fernandes Machado and V.S. Santana, *Catal. Today*, 2005, 107-108, 595–601.
6 M. Zeng, *Bull. Korean Chem. Soc.*, 2013, 34, 953–956.
7 M.S. Hook, P.G. Hartley and P.J. Thistlethwaite, *Langmuir*, 1999, 15, 6220–6225.